

## **Battle Damage Modeling**

**Capt. (Dr.) Ferdinando Dolce**

Italian Air Force – Flight Test Center – Chemistry Department  
“M. De Bernardi” AFB  
00040 Pomezia (Rome)  
Italy

[ferdinando.dolce@aeronautica.difesa.it](mailto:ferdinando.dolce@aeronautica.difesa.it)

### ***ABSTRACT***

Military structures are susceptible to high velocity impact due to both ballistic and blast loads. During a high velocity impact a shock wave much greater than static collapse resistance propagates through the material. Metallic structures usually undergo large plastic deformations absorbing impact energy before reaching equilibrium. Due to their high specific properties, also fiber-reinforced polymers are being considered for energy absorption applications in military armors. A deep insight into the relationship between projectile/explosion loads, composite architecture fracture behavior will offer the possibility to understand battle damage mechanics.

This work deals with 3D numerical simulations of damage on hybrid composite (ceramic/metal and glass/carbon fiber) plates subjected to ballistic and blast loads.

The simulation results are presented and compared with the experimental data, showing good agreement in terms of dynamic deflection, damage morphology and residual deformation.

### **1. INTRODUCTION**

Modern military systems are a compromise between the need of a great mobility and the increasing payload request [1]. These fairly opposite design requirements are leading the development of lightweight weapons and research into lightweight structures is playing an important role in this process. With the associated request for lighter protection systems, there has been an increasing move towards armor systems which are both structural and protection components at the same time. Analysis of material response at impulsive loads such as ballistic or blast impact, play a key role during this process and since the costs of experimental trials are usually very high, numerical Finite Element Method (FEM) simulations can be a useful tool in order to minimize the number of trials and also to understand general phenomenological behavior.

### **2. FEM SIMULATION OF HIGH VELOCITY IMPACT**

FEM consists of imaging a structural component to be composed of discrete parts (finite elements), which are then assembled in such a way as to represent the deformation of the structure under load [2]. The first step in FE analysis is called “mesh generation” where the real structural system (or a skilled simplified real system) is divided in a finite number of sub-systems of nodes and elements (Figure 1).

## Report Documentation Page

*Form Approved*  
*OMB No. 0704-0188*

Public reporting burden for the collection of information is estimated to average 1 hour per response, including the time for reviewing instructions, searching existing data sources, gathering and maintaining the data needed, and completing and reviewing the collection of information. Send comments regarding this burden estimate or any other aspect of this collection of information, including suggestions for reducing this burden, to Washington Headquarters Services, Directorate for Information Operations and Reports, 1215 Jefferson Davis Highway, Suite 1204, Arlington VA 22202-4302. Respondents should be aware that notwithstanding any other provision of law, no person shall be subject to a penalty for failing to comply with a collection of information if it does not display a currently valid OMB control number.

1. REPORT DATE <b>MAY 2010</b>	2. REPORT TYPE <b>N/A</b>	3. DATES COVERED <b>-</b>	
4. TITLE AND SUBTITLE <b>Battle Damage Modeling</b>		5a. CONTRACT NUMBER	
		5b. GRANT NUMBER	
		5c. PROGRAM ELEMENT NUMBER	
6. AUTHOR(S)		5d. PROJECT NUMBER	
		5e. TASK NUMBER	
		5f. WORK UNIT NUMBER	
7. PERFORMING ORGANIZATION NAME(S) AND ADDRESS(ES) <b>Italian Air Force Flight Test Center Chemistry Department M. De Bernardi AFB 00040 Pomezia (Rome) Italy</b>		8. PERFORMING ORGANIZATION REPORT NUMBER	
9. SPONSORING/MONITORING AGENCY NAME(S) AND ADDRESS(ES)		10. SPONSOR/MONITOR'S ACRONYM(S)	
		11. SPONSOR/MONITOR'S REPORT NUMBER(S)	
12. DISTRIBUTION/AVAILABILITY STATEMENT <b>Approved for public release, distribution unlimited</b>			
13. SUPPLEMENTARY NOTES <b>See also ADA564486. Battle Damage Repair Techniques and Procedures on Air Vehicles - Lessons Learned and Prospects. RTO-EN-AVT-156</b>			
14. ABSTRACT <b>Military structures are susceptible to high velocity impact due to both ballistic and blast loads. During a high velocity impact a shock wave much greater than static collapse resistance propagates through the material. Metallic structures usually undergo large plastic deformations absorbing impact energy before reaching equilibrium. Due to their high specific properties, also fiber-reinforced polymers are being considered for energy absorption applications in military armors. A deep insight into the relationship between projectile/explosion loads, composite architecture fracture behavior will offer the possibility to understand battle damage mechanics. This work deals with 3D numerical simulations of damage on hybrid composite (ceramic/metal and glass/carbon fiber) plates subjected to ballistic and blast loads. The simulation results are presented and compared with the experimental data, showing good agreement in terms of dynamic deflection, damage morphology and residual deformation.</b>			
15. SUBJECT TERMS			
16. SECURITY CLASSIFICATION OF:			17. LIMITATION OF ABSTRACT <b>SAR</b>
a. REPORT <b>unclassified</b>	b. ABSTRACT <b>unclassified</b>	c. THIS PAGE <b>unclassified</b>	
			18. NUMBER OF PAGES <b>16</b>
			19a. NAME OF RESPONSIBLE PERSON

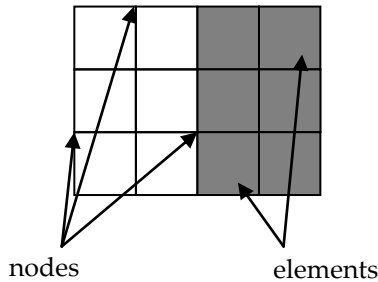


**Figure 1 – Nodes and elements (FEM)**

Each element has an assigned displacement field and part of FE modeler skill is in selecting appropriate elements of the correct size and distribution (FE mesh).

In structural analysis problems the response of a structure under load certainly depends on the intensity of applied load but also on the rate at which the load is applied. In general, the analysis of the response of a deformable body comes under two classes known as wave propagation problems or structural dynamics problems. Wave propagation problems are defined by loading that excites a large number of the structure’s highest natural frequency modes. When the load’s frequency is similar to the structure’s lowest natural frequency modes and the response is governed by inertia, the problem is called a structural dynamic problem. The first typology of problem concerns the ballistic and blast wave impact problems.

### **3. LAGRANGIAN AND EULERIAN APPROACH**

The configuration of a FE model, as well as how properties such as mass, energy and material strength are analyzed, is the main way of distinguishing between various models. Lagrangian and Eulerian are the two basic methods, which are both implemented in hydrocodes such as LS-DYNA. In a Lagrangian approach the mesh is created so that elements’ boundaries outline the free surfaces and material boundaries. Hence in this case the local reference system is “attached” to the structure’s body and it “follows” the structure’s displacements. In Lagrangian models the mesh will distort as much as the material will (Figure 2) and coordinates, velocities and forces are related with the corner nodes, while stresses, strains, pressures and energies are associated with the finite elements.

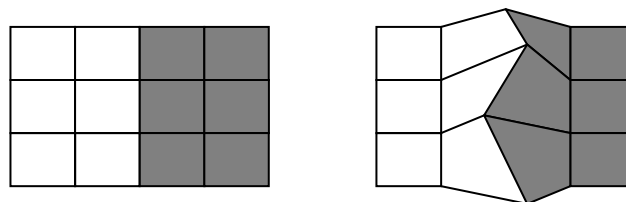


**Figure 2 – Example of Lagrangian FE model**

The main problems with Lagrange solvers occur when large deformations are involved. Severe distortion of the mesh can result in inaccuracies, negative densities and extremely small time-steps (Figure 3).

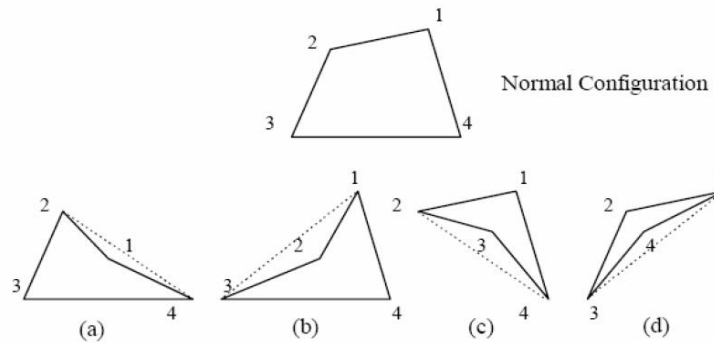


Figure 3 – Example of mesh distortion

In order to deal with this problem it can be necessary to manually redraw the mesh (“rezoning”) or eliminating distorted elements through erosion algorithms. Therefore they are typically not used for models that involve flow or large distortion, although Lagrangian approach is often used in impact models where two solid objects collide, as both target and projectile.

The Eulerian approach differs from Lagrangian approach in a few fundamental concepts. First of all instead of confining the grid to the structural component, Eulerian models place a grid over the space in which the materials can move. As the FE analysis progresses the component will move while the mesh remains motionless (Figure 4). Individual nodes and cells basically “observe” as the model flows by. In a typical Euler model, the centers of the cells are used as interpolation points for all variables. In Eulerian model the material moves through a computational mesh that is fixed in space and each element is allowed to contain a number of different materials. The main problems with Eulerian formulation are the amount of elements that Eulerian model require and their poor handling of geometry. Since you are not only modeling the object of interest, but the space around that object, more elements and therefore more memory and time can be required than a standard Lagrange model. Also since the mesh does not distort with the observed material, it becomes more difficult to track the various components of a part, and therefore observe a single piece evolution. Therefore Eulerian models are typically not used to model solid objects. The advantage of Euler solvers is that they do not deform and therefore are not subject to the limitations imposed by deformation in Lagrange solvers. They can also allow the mixing of different materials inside the elements. Therefore the shape of material surfaces is not completely limited by element size. They are used when a problem involves high levels of deformation or fluid flow (i.e. gases and liquids), while Lagrangian solvers are normally used to model solids that do not experience such large deformations.

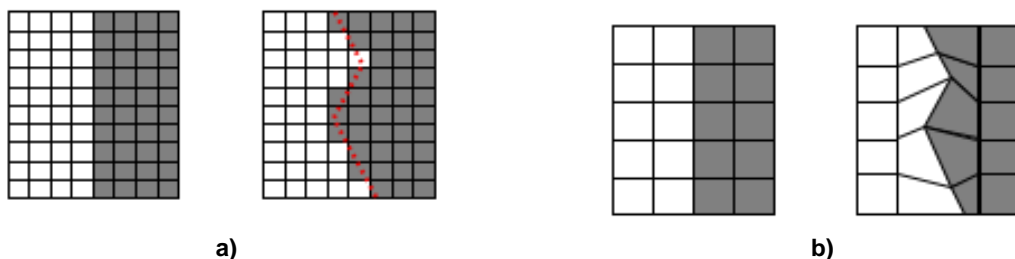


Figure 4 – Example of FE Eulerian model (a) compared with a FE Lagrangian model (b)

Hydrocodes such as LS-DYNA make use of a set of equations called equations of state (EOS). An EOS relates the density (or volume) and internal energy (or temperature) of the material with

pressure [3] by applying the principles of conservation of mass, momentum and energy. For example, uniform gas would typically be modeled with an EOS based on the Ideal Gas Law. Other functions (constitutive relationships) describe the material behavior by relating stress and strain, such as strain-rate, work hardening and thermal softening laws. Using these relationships, the FE code advances the calculation forward for a very short period, called time-step, and then performs again the same sequence of calculation. Since the time-step is an important variable, the commercial FE code has an algorithm to determinate this parameter. This subroutine needs many inputs, such as the speed of sound in the material, the FE size mesh and the safety factor, which prevents that the time-step becomes too large [4]. Smaller safety factors result in smaller time-steps and therefore more accurate solutions. However, smaller time-steps will require more calculations to reach the termination time. Therefore in hydrocodes algorithms element size not only determines the complexity of the problem spatially but temporally as well.

## 4. CASE STUDIES

### 4.1 Ballistic impact model

Before modeling ballistic impact, materials dynamic behavior has been verified through a Flyer Plate Impact Test (FPIT). The FPIT is a technique used to study dynamic behavior of materials and to obtain their equation of state. During this test two thin discs are subjected to impact in a gas gun and velocity evolution with time at the sample plate rear surface is measured (figure 5).

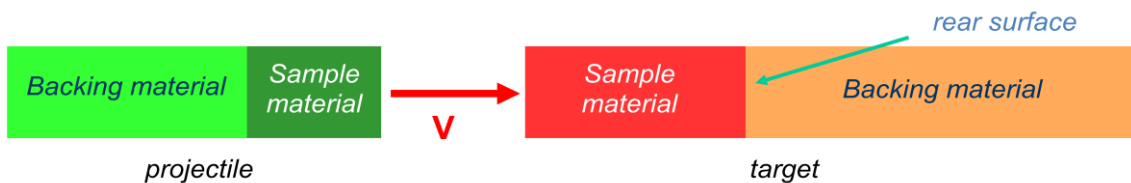


Figure 5 – FPIT scheme

This signal can show specific features that can be used to compare with numerical predictions in order to check both constitutive and damage model performance (figure 6).

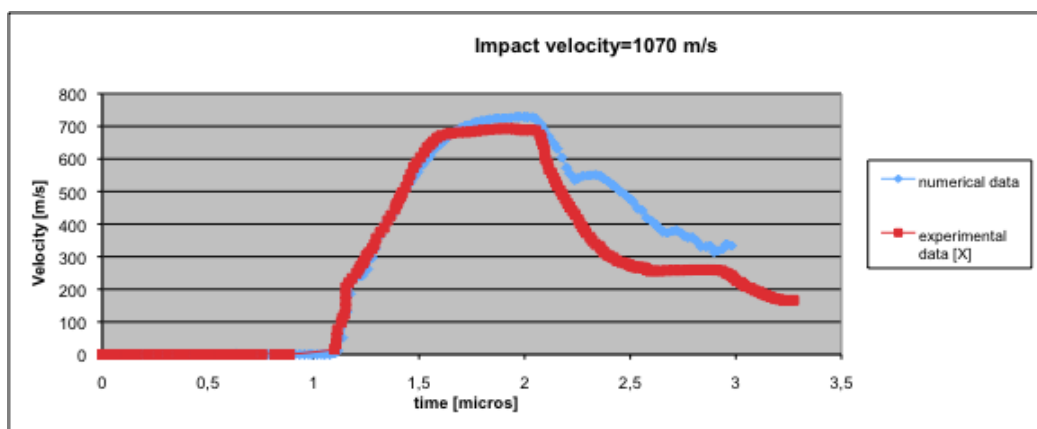


Figure 6 – FPIT results

After FPIT, ballistic impact models have been generated [5] where a projectile impacts at 1.52 and 1.79 Km/s against three different target configurations (figure 7).

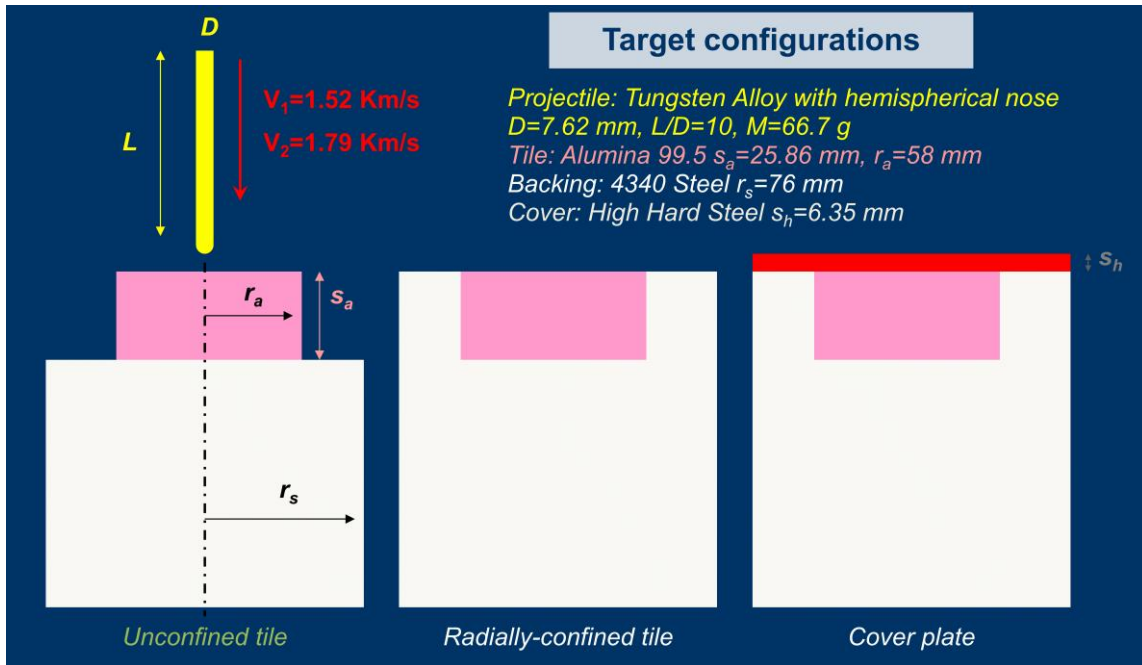


Figure 7 – Target configuration

Some of the numerical results are represented in figure 8 whilst in figure 9 are compared experimental [6] and numerical results in terms of penetration/projectile length ratio.

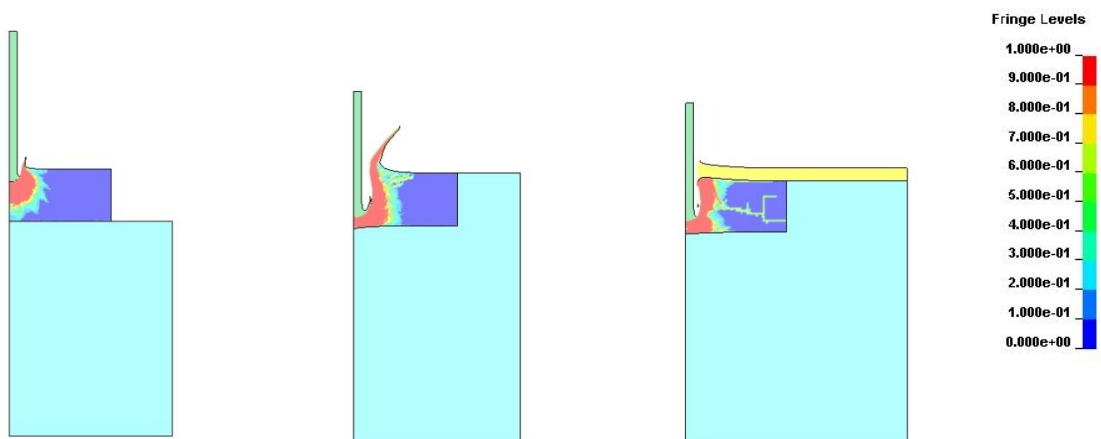


Figure 8 – Ballistic model numerical results

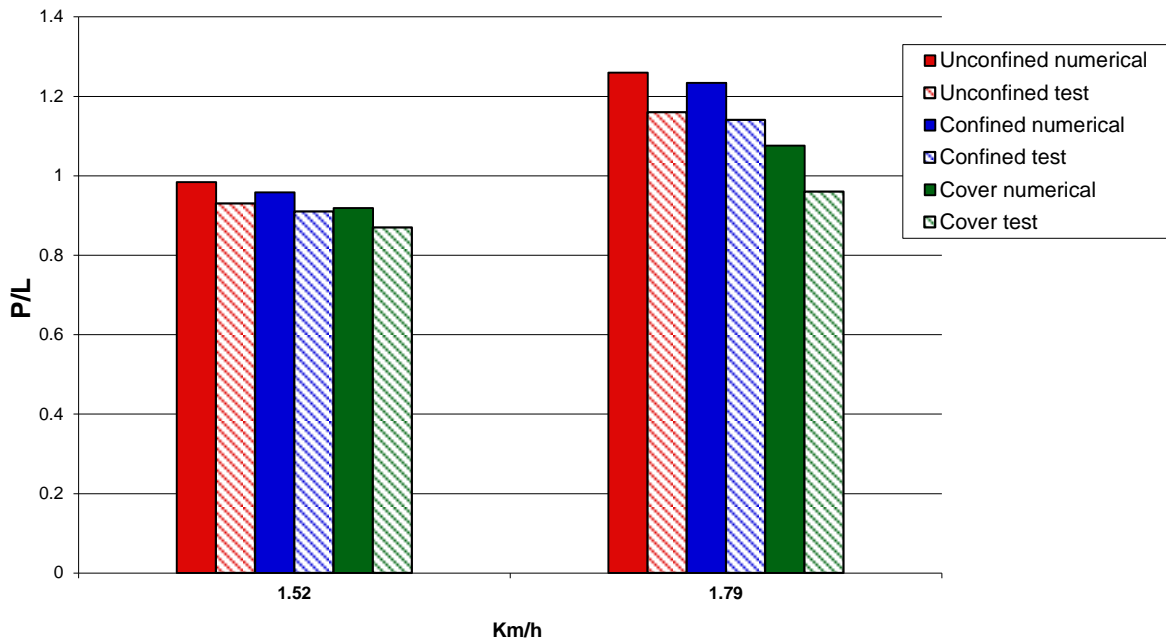


Figure 9 – experimental-numerical results

#### 4.2 Blast impact model

Blast impact models simulated blast trials performed with charge at a stand-off distance of 150 mm on 800x800 mm square targets clamped in position using a purpose built test rig [7]. The explosive selected was the C-4 (Composition 4) that is a common military plastic explosive. The trials were performed on different materials targets. In order to assess the numerical model capability, test and simulations have been first carried out on steel Rolled Homogenous Armors (RHA) of different thickness loaded by increasing C-4 charges [8], since metals behavior under blast load is better understood and easier to model than composites. Hence experimental and numerical response of quasi isotropic composite laminates, carbon fiber (Tenax STS 24k NCF) in standard epoxy matrix ( $\pm 45/90,0$ )<sub>7s</sub>, 27 mm thick and loaded by 750g and 825g C-4 charges has been analyzed and discussed. For all the composite panels under assessment, delamination was found with the most extensive affected area occurring midway through the thickness (Figure 10a). This is largely to be expected, since the mid-plane of the panel corresponds to the neutral axis under bending. The damage observed in failed tests did not correspond to a hole in the target (Figure 10b). In order to assess damage through the laminates thickness a reservoir of water was placed on top (rear) surface of the plates and the panel was examined for water leakage.



a



b

Figure 10 – Details of delamination damage at 750g C-4 (a) and rear face condition after blast impact at 825g C-4 (b)

#### 4.2.1 FE model

The FE models were made of three components: frame, bolts and target (Figure 11).

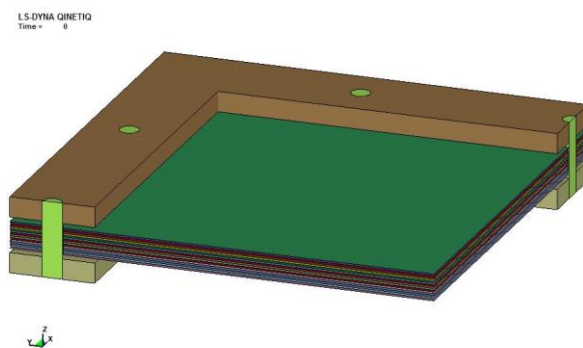


Figure 11 – Composite FEM model

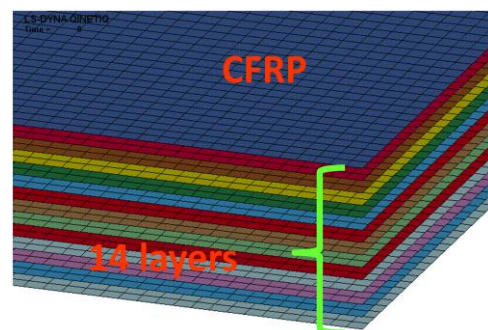


Figure 12 – CFRP: 14 layers with 4 integration point for each ply ( $\pm 45/90,0$ )<sub>7s</sub>

The simulation was performed with the commercial FEM code LS-DYNA.

Fixed boundary conditions were applied on the lower surface of frame in order to simulate the rest of the basement and symmetry boundary conditions were applied on the nodes lying on plane XZ and YZ. The contacts between target and bolts and between target and frame were modeled through the \*CONTACT AUTOMATIC NODES TO SURFACE. Besides, confining nodes of bolts and frame were merged, hence no contact card was applied between these components.

On the metallic targets two approaches were used to simulate the blast load: a simply Lagrangian model with CONWEP [9] load function and a Multi Material Arbitrary Eulerian Lagrangian (MMALE) model. Both shell and solid elements were used to simulate the metallic plate.

A multi-layers shell element with interface delamination model was generated to simulate the composite target. Only 14 layers were modeled instead of the 56 layers that really make the panel in order to avoid a too high number of elements. Hence one layer was made of four integration points and each of them is associated to a different layer ( $\pm 45/90,0$ ) (Figure 12). The total number of elements for the composite model is about 169.000 with a size mesh of about 2.6 mm.

Belytschko-Tsay under-integrated formulation was applied to composite shell elements. Hourglass viscous form control was applied to under-integrated shell elements with an hourglass coefficient of  $1e^{-3}$ . The CFRP models represented in Table 1 were simulated.

**Table 1**

Charge weight	600	750	825	863	900
CFRP	✓	✓ ✓	X		X
	✓ Passed test	x failed test		■ performed FEM simulation	

**4.2.2 Constitutive Material Models and Properties**

The RHA target was modeled with the Johnson-Cook (J-C) material model [10] that is implemented in LS-DYNA with \*MAT\_015 card. In equation (1)  $\epsilon$  is the effective plastic strain,  $\dot{\epsilon}$  is the total strain rate,  $\dot{\epsilon}_0$  is the reference plastic strain rate, T is the temperature of the work material T<sub>m</sub> is the melting temperature of the work material and T<sub>room</sub> is the room temperature. Coefficient A is the strain hardening constant, B is the strain hardening coefficient, C is the strain rate coefficient, n is the strain hardening exponent and m is the thermal softening exponent.

$$\sigma_y = (A + B\epsilon^n) \left( 1 + C \ln \left( \frac{\dot{\epsilon}}{\dot{\epsilon}_0} \right) \right) \left( 1 - \left( \frac{T - T_{room}}{T_m - T_{room}} \right)^m \right) \quad (1)$$

The strain at fracture is given by:

$$\epsilon^f = \left[ D_1 + D_2 e^{D_3 \sigma^*} \right] \left[ 1 + D_4 \ln \dot{\epsilon}^* \right] \left[ 1 + D_5 \left( \frac{T - T_{room}}{T_m - T_{room}} \right) \right] \quad (2)$$

here  $\sigma^*$  is the ratio of pressure divided by effective stress ( $\sigma^* = p / \sigma_{eff}$ ) and  $\dot{\epsilon}^*$  is the ratio of effective total strain rate normalized by reference plastic strain rate. Fracture occurs when the damage

$$D = \sum \frac{\Delta \epsilon}{\epsilon^f}$$

parameter reaches the value of 1.

When dealing with solid elements, the J-C LS-DYNA model requires an equation of state (EOS). In this case, the EOS chosen is the Gruneisen equations (3) and (4).

$$p = \frac{\rho_0 C^2 \mu \left[ 1 + \left( 1 - \frac{\gamma_0}{2} \right) \mu - \frac{\alpha}{2} \mu^2 \right]}{\left[ 1 - (S_1 - 1) \mu - S_2 \frac{\mu^2}{\mu + 1} - S_3 \frac{\mu^3}{(\mu + 1)^2} \right]^2} + (\gamma_0 + \alpha \mu) E \quad (3)$$

*compressed materials*

$$p = \rho_0 C^2 \mu + (\gamma_0 + \alpha \mu) E \quad (4)$$

*expanded materials*

The composite material behavior was modeled with \*MAT\_54 (ENHANCED\_COMPOSITE\_DAMAGE) valid only for shell element formulation. This card is the enhanced version of \*MAT\_22 and it models arbitrary orthotropic materials such as unidirectional layers in composite material shell structures. In this work the Chang and Chang failure criterion was applied and laminated shell theory was activated to properly model the transverse shear deformation. A delamination model was applied between each shell layers interface. The model works through the contact tiebreak formulation [11] and, being a contact algorithm, it does not need elements definition. Tie-break contact allows the modelling of connections, which transmits both compressive and tensile forces with optional failure criteria. Before failure, tie-break contact works both in tension and compression. After failure, this contact behaves as a surface-to-surface contact with thickness offsets. Hence, after failure, no interface tension is possible. Different tie-break failure criteria can be defined. With option 9 it can be defined a failure criteria that is an extension of Dycoss Discrete Crack Model [12] based on the fracture model defined in the cohesive material model: \*MAT\_138 (COHESIVE\_MIXED\_MODE). This card includes a bilinear traction-separation law with quadratic mixed mode delamination criterion and a damage formulation [13]. In the interface cohesive model the ultimate displacements in the normal and tangential directions are the displacements at the time when the material has failed completely. The bilinear traction-separation law gives a linear stiffness for loading followed by the linear softening during the damage and provides a simple relationship between the energy release rates, the peak tractions and the ultimate displacements:

$$G_{IC} = \frac{T \cdot UND}{2} \quad G_{IIC} = \frac{S \cdot UTD}{2} \quad (5)$$

where T is the peak traction in normal direction, S is the peak traction in tangential direction, UND is the ultimate displacement in the normal direction, UTD is the ultimate displacement in the tangential direction,  $G_{IC}$  is the Mode I energy release,  $G_{IIC}$  is the Mode II energy release.

If the peak tractions are not specified, they can be computed from the ultimate displacements. In the cohesive material model, the total mixed-mode relative displacement  $\delta_m$  is defined as  $\delta_m = \sqrt{\delta_I^2 + \delta_{II}^2}$ , where  $\delta_I = \delta_3$  is the separation in normal direction (Mode I) and  $\delta_{II} = \sqrt{\delta_1^2 + \delta_2^2}$  is the separation in tangential direction (Mode II). The mixed-mode damage initiation displacement  $\delta_0$  (onset of softening) is given by:

$$\delta^0 = \delta_I^0 \delta_{II}^0 \sqrt{\frac{1 + \beta^2}{(\delta_{II}^0)^2 + (\beta \delta_I^0)^2}} \quad (6)$$

where  $\delta_{I0} = T/EN$  and  $\delta_{II0} = S/ET$  are the single mode damage initiation separation, EN is the stiffness normal to the interface plane, ET is the stiffness into the interface plane and  $\beta$  is the “mode mixity”. The ultimate mixed-mode displacement  $\delta_F$  (total failure) for the Benzeggagh-

Kenane law is:

$$\delta^f = \frac{2}{\delta^0 \left( \frac{1}{1+\beta^2} EN + \frac{\beta^2}{1+\beta^2} ET \right)} \left[ G_{IC} + (G_{IIC} - G_{IC}) \left( \frac{\beta^2 ET}{EN + \beta^2 ET} \right)^{XMU} \right] \quad (7)$$

where XMU is the exponent of the mixed-mode criteria.

### 4.2.3 MMALE blast model

To model blast pressure, a MMALE approach was employed (Figure 13). Explosive and air mesh need to be generated into the FE model. The interface between Eulerian ambient (air + explosive) and Lagrangian structure (target) also needs to be defined.

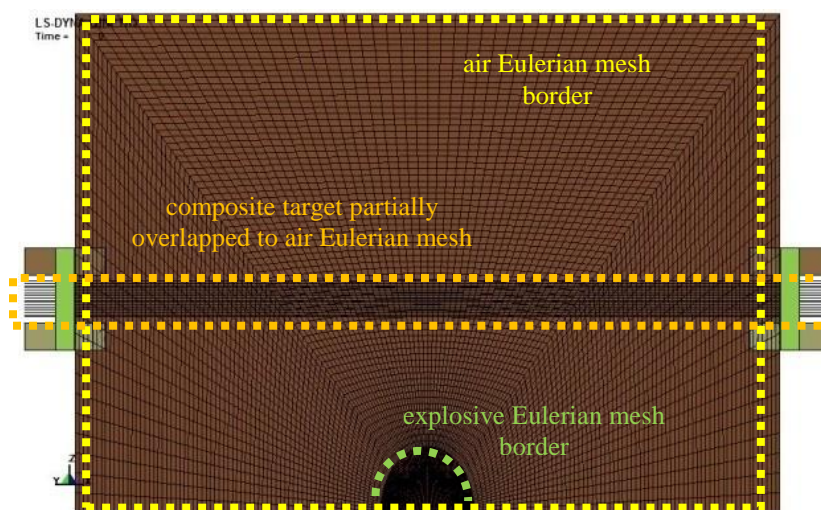


Figure 13 – MMALE model

Eulerian ambient was modeled with 1 point MMALE solid element with ambient pressure outflow option in order to allow the fluid flowing outside the mesh boundaries. Symmetry boundary conditions were guaranteed by the slip condition applied to symmetry plane YZ and XZ (fluid flow's normal component equal to zero). The number of Eulerian elements was about 171.000. To model air and explosive material behaviors \*MAT\_009 (NULL) and \*MAT\_008 (HIGH\_EXPLOSIVE\_BURN) were used respectively. These cards require an EOS: for the air was used a linear polynomial EOS, while for the explosive the JWL EOS. The contact between the fluid flow and the target can be modeled in LS-DYNA through a specific card called \*CONSTRAINED\_LAGRANGE\_IN\_SOLID that provides the coupling mechanism for modeling Fluid-Structure Interaction (FSI). In the case of the composite structures an FSI card was defined for each ply giving a total number of 14 FSI cards in order to guarantee the interaction also in the case of through thickness shells composite failure (Figure 14).

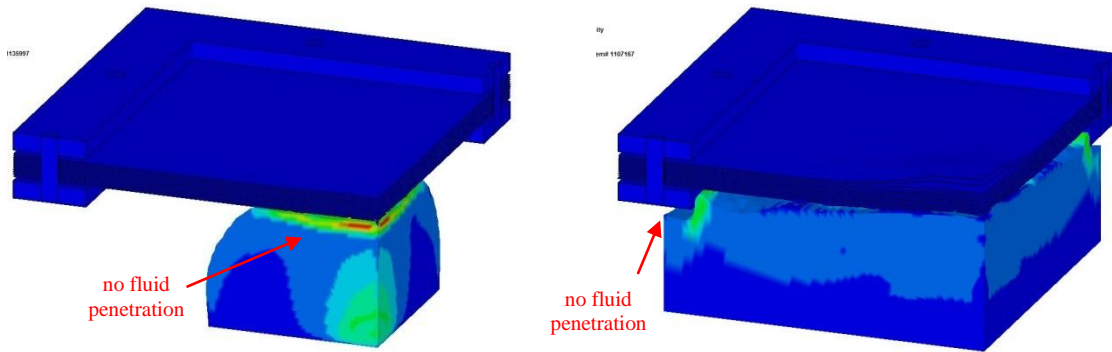


Figure 14 – Fluid-Structure Interaction

#### 4.2.4 Results

In general, during blast loading on panels a compressive stress wave within the material is generated by the impact of pressure wave at the front face of the target. This compressive wave propagates throughout the material until it reaches the rear surface of target, where it is reflected as a tensile wave. In the following figures, some of the results obtained on metallic plates are illustrated in terms of dynamic deflection and residual deformation, showing a very good agreement (Figures 15-17) [7].

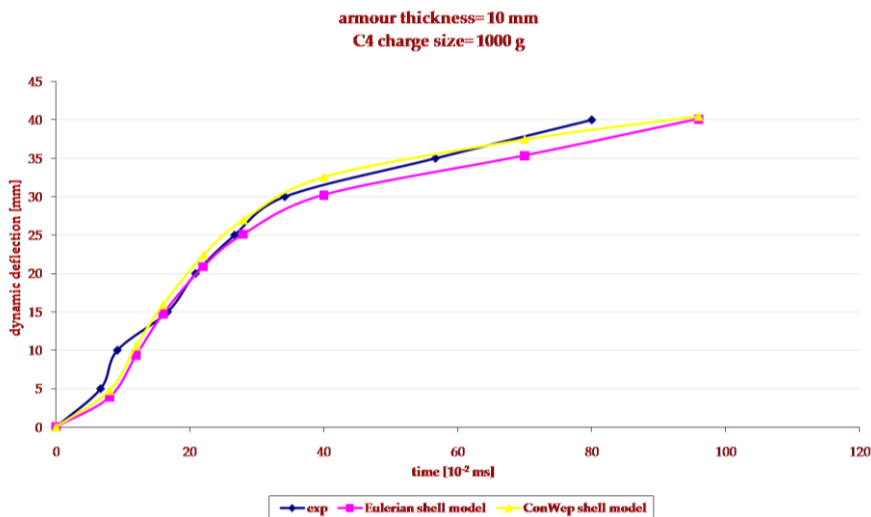


Figure 15 – Dynamic deflection steel RHA (10 mm 1000 g)

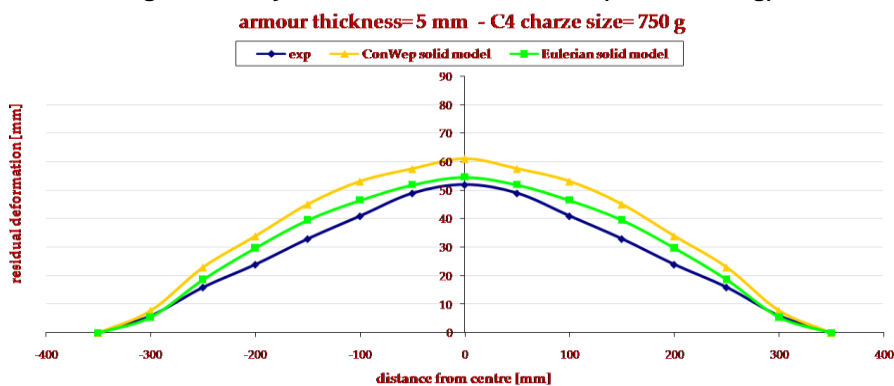


Figure 16 – Residual deflection steel RHA (5 mm 750 g)

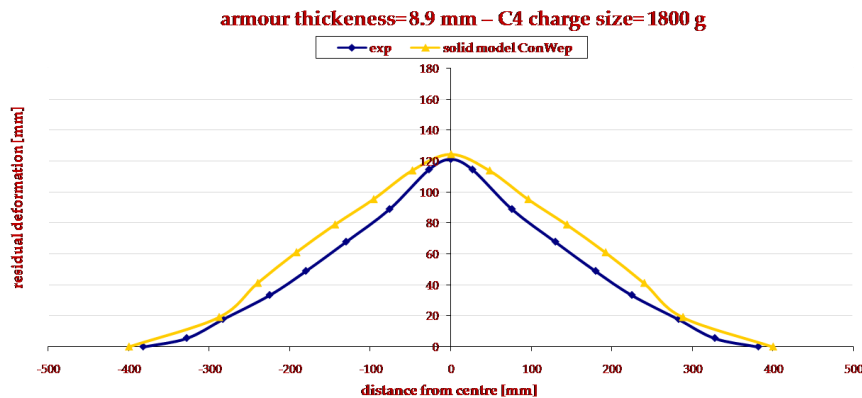


Figure 17 – Residual deflection steel RHA (8.9 mm 1800 g)

In the composite material laminate, the initial compressive stresses may produce some degree crushing failure in the composite matrix. According to the geometry and boundary conditions for laminate plates, the tensile reflected wave produces an extensive delamination between the last plies of the laminate. In the following instants, the pressure on the target distributes on the whole material and generates a bending load on the panel, which can also lead to fibre breakage.

In Figure 18 is illustrated numerical dynamic deflection compared with experimental measure [14]. If in the first instants of deflection numerical model appears fairly over-stiff, the steady-state response tends to the same deflection value and rate.

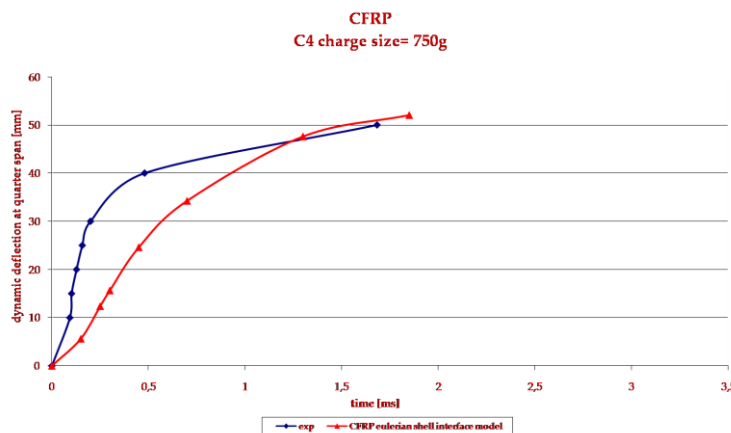
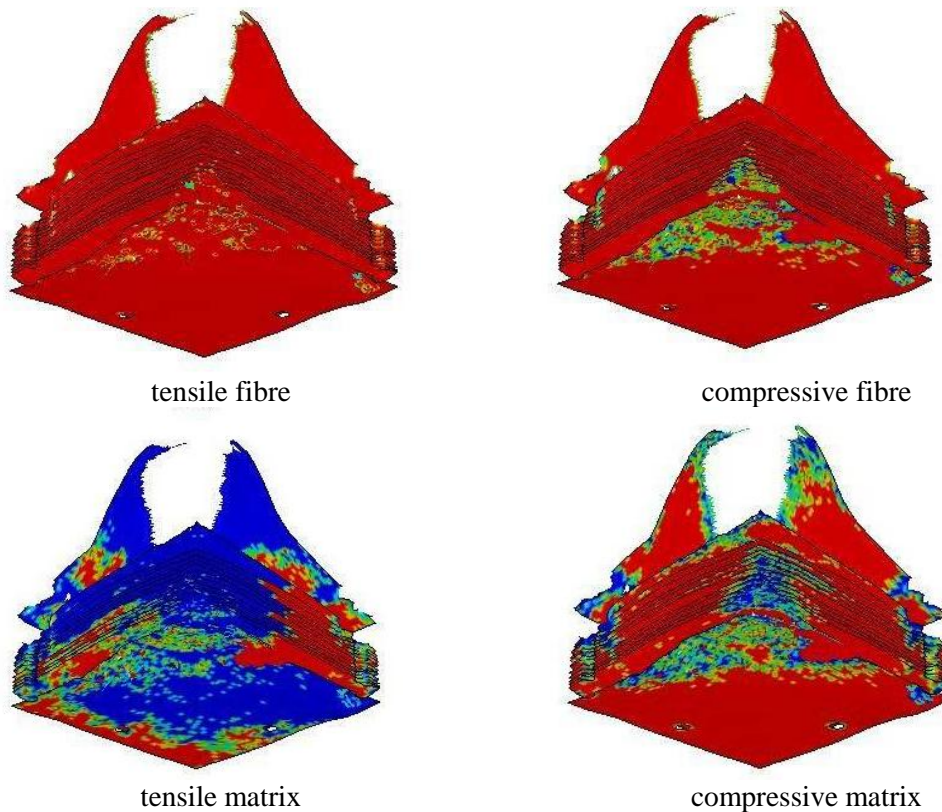
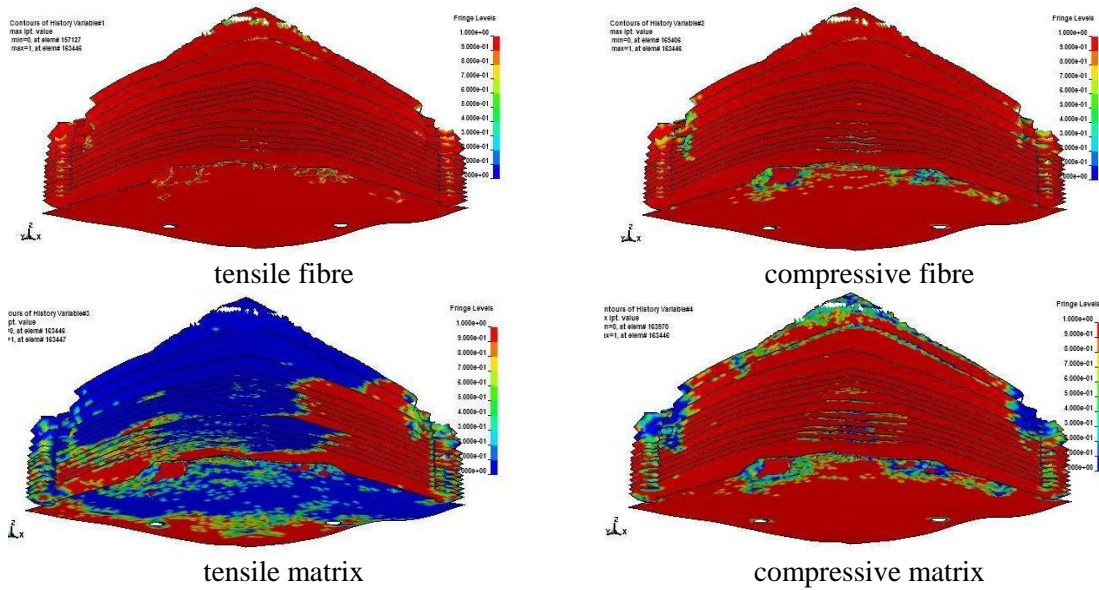


Figure 18 – Dynamic deflection CFRP (750 g)

In figures 19 and 20 damage map results are reported. The damage maps represent the composite failure distribution, split in fiber/matrix and tension/compression damages. In the maps damage is maximum if it is equal to 0 (blue regions), minimum if it is equal to 1 (red regions). Each element is removed by LS-DYNA when the damage is equal to 0 in all its own integration points. Maximum integration point values (conservative condition) are illustrated in exploded view (z direction - factor 2) to better visualize the damage in each ply.

The experimental damage assessment performed after blast tests was not possible to numerically perform through the approach used in this work. In consideration that the damage assessment plays a key role in the comparison process of numerical and experimental results, a numerical failure criterion different from the experimental one was defined in order to evaluate model prediction

capability. The matrix failure, both in tension and in compression, was the numerical damage assessment criterion selected. In fact, the water penetration through the panel thickness of experimental damage assessment can be much more easily associated to matrix failure rather than to fibers breakage.



The compressive matrix damage zone was found along the whole central thickness for CFRP models only in the case of 875 g blast load, while is almost absent in the case of 750 g blast load. This agrees very well with the experimental data showing that the composite panel was not able to resist to the considered blast load as found during the experimental campaign. Finally, in figures 21 and 22 numerical results are also compared with provided real damage morphology [14] showing a fairly good agreement.

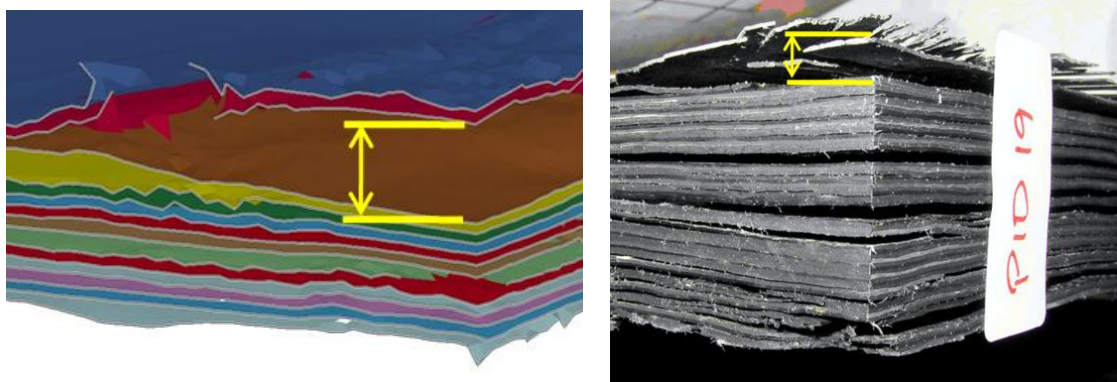


Figure 21 – CFRP delamination

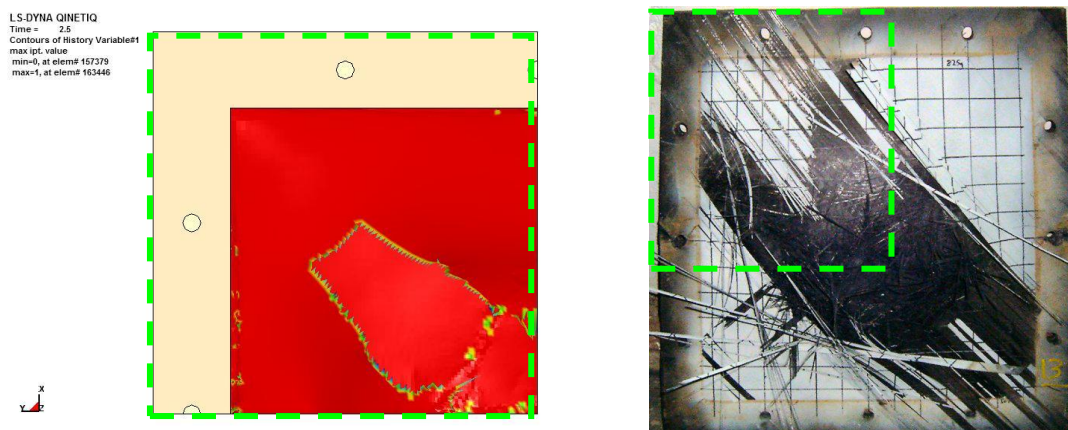


Figure 22 – CFRP rear damage

## ACKNOWLEDGEMENTS

The author would like to gratefully acknowledge the support of QinetiQ for the fundamental data provided to realize this study, Prof. N. Bonora, Dr. M. Meo, L.T.Col. M. Bernabei and Maj. L. Aiello for the special effort offered to realize this work.

## BIBLIOGRAPHY

- [1] Remennikov, A.M., A review of methods for predicting bomb blast effects on buildings. *Journal of Battlefield Technology*, 2003. 6(3): p. 5-10.
- [2] Matthews, F.L., et al., *Finite element modelling of composite and structures*. 2000, Abington: Woodhead Publishing Limited.

- [3] Anderson, J.C.E., An overview of the theory of hydrocodes. *International Journal of Impact Engineering*, 1987. 5(1-4): p. 33-59.
- [4] Zukas, J.A., *Introduction to hydrocodes*. 2004, Amsterdam: Elsevier.
- [5] Dolce, F., *Analisi del danno da impatto ad alta velocità su strutture composite in alumina*. PhD thesis, University of Cassino (IT), 2007.
- [6] Anderson Jr. C.E., Royal-Timmons S.A., Ballistic performance of confined 99.5%  $Al_2O_3$  ceramic tiles. *Int. J. Impact Engng*, Vol. 19, No. 8, pp. 703-713, 1997.
- [7] Wright, A.J., *EUROPA CAFV Programme - Numerical Modelling Study*. 2006, QinetiQ.
- [8] Dolce, F., *Blast impact simulation on composite military armors*. MPhil thesis, University of Bath (UK), 2009.
- [9] Hyde, D.W., *CONWEP: Conventional Weapons Effects Program*. 1991: US Army Engineer Waterways Experiment Station, USA.
- [10] Johnson, G.R. and W.H. Cook, Fracture characteristics of three metals subjected to various strains, strain rates, temperatures and pressures. *Engineering Fracture Mechanics*, 1985. 21(1): p. 31-48.
- [11] Bala, S., *Tie-Break Contacts in LS-DYNA*, Livermore Software.
- [12] Lemmen, P.P.M. and G.J. Meijer, *Failure Prediction Tool Theory and User Manual*. 2001, TNO Report.
- [13] *LS-DYNA keyword user's manual - Vol. I-II*, v. 971, Editor. 2007, Livermore Software Technology Corporation (LSTC).

